Available online at www.sciencedirect.com

ScienceDirect

Computer Aided Geometric Design 25 (2008) 137–147

COMPUTER AIDED GEOMETRIC DESIGN

www.elsevier.com/locate/cagd

Local energy-optimizing subdivision algorithms

I. Ginkel, G. Umlauf *

Geometric Algorithms Group, Department of Computer Science, University of Kaiserslautern, D-67653 Kaiserslautern, Germany

Received 12 April 2007; received in revised form 27 July 2007; accepted 15 August 2007

Available online 15 September 2007

Abstract

In this paper a method is presented to fair the limit surface of a subdivision algorithm locally around an extraordinary point. The dominant six eigenvalues of the subdivision matrix have to satisfy linear and quadratic equality- and inequality-constraints in order to guarantee normal-continuity and bounded curvature at the extraordinary point. All other eigenvalues can be chosen arbitrarily within certain intervals and therefore can be used to optimize the shape of the subdivision surface by minimizing quadratic energy functionals. Additionally, if the sub- and subsub-dominant eigenvalues vary within predefined intervals, C^1-regularity of the surface and locality of the stencils can be guaranteed, although eigenvectors are changed.

Keywords: Subdivision algorithms; Algorithm of Loop; Algorithm of Catmull–Clark; Constrained optimization; Eigenvalues; Thin-plate energy

1. Introduction

A subdivision algorithm is an iterative technique to generate a sequence of ever finer control nets that converges to a so-called subdivision surface of arbitrary topology. Despite their simplicity subdivision surfaces are not widely used in CAD applications partially because they can have artifacts (Sabin and Barthe, 2003; Karciauskas et al., 2004). Although most subdivision surfaces are proved to be regular and normal-continuous everywhere, their shape may still be unsatisfactory. For example, the subdivision algorithms of Catmull–Clark (Catmull and Clark, 1978) or Loop (Loop, 1987) cannot generate surfaces with convex extraordinary points for large valences (Karciauskas et al., 2004). Even worse, naive approaches to overcome this situation may generate so-called hybrid surfaces where positive and negative Gauss curvatures appear in every infinitesimal small neighborhood of an extraordinary point.

For linear subdivision algorithms a subdivision matrix maps coarse to fine control nets. It was already observed in Doo and Sabin (1978) that the eigenvalues and eigenvectors of the subdivision matrix control the continuity of the subdivision surface around extraordinary points. This was later made precise in Reif (1995), Prautzsch (1998), Zorin (1998). The linear combinations encoded in the rows of the subdivision matrix are conveniently represented by stencils. They show graphically which points of a coarse control net are linearly combined to compute a point of a fine control net. For example the stencils of the algorithm of Loop (Loop, 1987) are shown in Fig. 1.

[*] Corresponding author.
E-mail addresses: ginkel@informatik.uni-kl.de (I. Ginkel), umlauf@informatik.uni-kl.de (G. Umlauf).

0167-8396/$ – see front matter © 2007 Elsevier B.V. All rights reserved.
doi:10.1016/j.cagd.2007.08.003

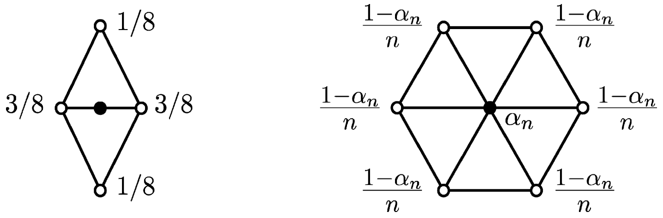

Fig. 1. The stencils of the algorithm of Loop with $\alpha_6 = 5/8$ and $1 - c < 4\alpha_n < 4 + c$, $c := \cos(2\pi/n)$.

The simplest approach to improve the shape of a subdivision surface is to use the free parameters in the stencils (cf. Fig. 1). This was already done in the first publications about subdivision surfaces (see e.g. Catmull and Clark, 1978; Loop, 1987). The next approach to tune the behavior of the curvature at extraordinary points aimed at bounded or zero Gauss curvature at extraordinary points (Holt, 1996; Loop, 2002; Ni et al., 2007; Prautzsch and Umlauf, 1998; Prautzsch and Umlauf, 2000; Sabin, 1991). Here, the eigenvalues of the subdivision matrix are changed such that the necessary conditions for bounded or zero Gauss curvature are satisfied while the number and size of affected stencils stays small.

For subdivision surfaces with bounded Gauss curvature of arbitrary sign, i.e. allowing for hyperbolic and elliptic shapes, more advanced techniques must be used. In Barthe and Kobbelt (2004) also the eigenvectors are considered by computing the stencils in an optimization process. The resulting subdivision algorithms approximate the desired eigenvector behavior. Based on the analysis in Karciauskas et al. (2004), Peters and Reif (2004) a different approach is presented in Augsdörfer et al. (2005). Here, the eigenvalues are determined such that the necessary conditions for bounded Gauss curvature are satisfied and the variation of curvature of the central surfaces in the shape chart (cf. Peters and Reif, 2004) is minimized. This is a non-linear optimization process which can only be approximated. It leads to subdivision algorithms with eigenvalues that approximately minimize variation of Gauss curvature. Instead of changing the eigenstructure of the subdivision algorithm also the eigencoefficients of the control nets can be changed. This is done in Ginkel and Umlauf (2006) yielding a subdivision method for subdivision surfaces with bounded Gauss curvature of arbitrarily prescribed sign.

Of a different type are the approaches taken in Halstead et al. (1993), Kobbelt (1996). They do not tune the respective subdivision algorithms but also integrate optimization into the subdivision algorithm. The points of the fine control nets are computed such that a local or global energy functional is minimized. This requires the solution of a global system of linear equations.

In this paper we take an approach briefly mentioned in Prautzsch and Umlauf (2000). The eigenvalues of any stationary, linear and symmetric subdivision algorithm can be changed to satisfy the necessary conditions for bounded Gauss curvature using the technique described in Prautzsch and Umlauf (2000). This imposes equality- and inequality-constraints on the dominant six eigenvalues of the subdivision matrix. The remaining eigenvalues can be chosen arbitrarily and may be used for optimization as long as they have smaller modulus than the dominant six eigenvalues. Additionally, the inequality constraints allow the sub- and subsub-dominant eigenvalues to vary within predefined intervals. Then, a quadratic equation with linear and quadratic constraints is minimized to locally adapt the eigenvalues to the data, because the stencils depend linearly on the eigenvalues and a quadratic energy functional like the thin-plate energy depends quadratically on the control points. An example of this approach is presented in Ginkel and Umlauf (2007b), where the technique is briefly outlined for the algorithm of Catmull–Clark.

In this paper we describe the general technique, applicable to any stationary, linear and symmetric subdivision algorithm. This technique results in an algorithm which is non-stationary during a finite number of subdivision steps where the stencils generate the new control points such that the corresponding surface rings minimize a quadratic energy functional. When the energy improvement is below a pre-defined value the algorithm becomes stationary. The choice for the sub- and subsub-dominant eigenvalue of the last optimization step is then chosen for all subsequent subdivision steps, resulting in a stationary algorithm similar to the bounded curvature variant of the algorithm of Loop in Ginkel and Umlauf (2006).

In the following six sections we first outline the general setting and notation of subdivision surfaces and their analysis (Section 2). In Section 3 the tuning method and its relation to the Fourier analysis of the subdivision matrix are presented. This is used for energy minimization in Section 4. In Section 5 locality is proved, the effects of the minimization on the characteristic map are discussed and bounds for the sub-dominant eigenvalue are given guaranteeing

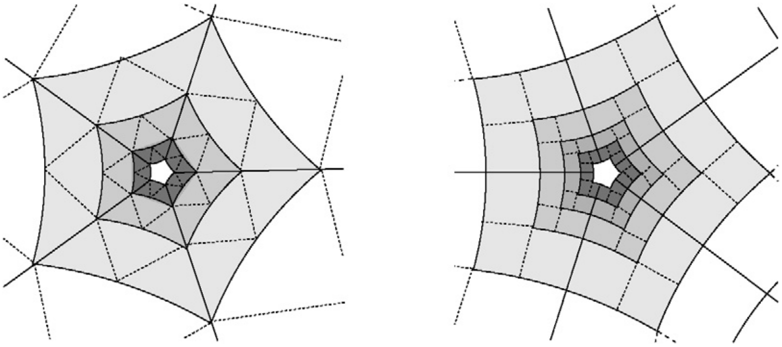

Fig. 2. Sequence of spline rings $\mathbf{x}_r$ for triangular meshes (left) and quadrilateral meshes (right).

a regular, injective characteristic map. The results of our method applied to the algorithms of Loop and Catmull–Clark are shown in Sections 6 and 7.

2. The subdivision setting

A linear subdivision algorithm computes from a coarse initial net of control points C_0, where a central point $\mathbf{c}_0$ of valence n is surrounded by k rings of regular control points, a refined net of control points C_1 of the same topology and with the same fixed number of points. This process is iterated to generate a sequence of control nets (C_r) with central point $\mathbf{c}_r$, where each control net C_r defines a spline ring $\mathbf{x}_r$. For subdivision algorithms such as the algorithms of Loop and Catmull–Clark, in the vicinity of an extraordinary point with valence $n \geqslant 3$ the subdivision surface $\mathbf{x}$ is the union of the extraordinary point $\mathbf{s}$ and the sequence of the spline rings

$$\bigcup_{r\in\mathbb{N}_0} \mathbf{x}_r(\Omega_n) \cup \mathbf{s} = \mathbf{x}$$

with $\mathbf{x}_r : \Omega_n \to \mathbb{R}^3$ and $\Omega_n := \Sigma \times \mathbb{Z}_n$, where $\Sigma := \{(u, v) \mid u, v \geqslant 0, 1 \leqslant u + v \leqslant 2\}$ for triangular nets and $\Sigma := [0, 2]^2 \setminus [0, 1)^2$ for quadrilateral nets, as illustrated in Fig. 2. Each surface ring is a linear combination of real valued functions $\mathbf{f}_0, \dots, \mathbf{f}_l$ defined on Ω_n with spatial control points $\mathbf{c}_r^0, \dots, \mathbf{c}_r^l \in \mathbb{R}^3$. Collecting the functions in a row vector $\mathbf{f}$, the sequence of control points is generated by iterated application of a square subdivision matrix S such that

$$C_r = S^r C_0, \quad \text{and} \quad \mathbf{x}_r = \mathbf{f} S^r C_0.$$

The eigenvalues $\lambda_0, \dots, \lambda_l$ of the subdivision matrix S are assumed to be real and ordered by modulus such that

$$1 = \lambda_0 > \underbrace{\lambda_1 = \lambda_2}_{=:\,\lambda} > \underbrace{\lambda_3 = \lambda_4 = \lambda_5}_{=:\,\mu} > |\lambda_6| \geqslant \dots \geqslant |\lambda_l| \qquad \text{(i)}$$

with corresponding eigenvectors $\mathbf{v}_0, \dots, \mathbf{v}_l$. For the subdivision surface to be C^1-regular with bounded Gauss curvature at $\mathbf{s}$ the following conditions are sufficient (see e.g. Reif, 1995; Peters and Umlauf, 2000):

(ii) $\mu = \lambda^2$, and
(iii) the characteristic map $\mathbf{f} \cdot [\mathbf{v}_1 \mathbf{v}_2]$ is regular and injective.

Note that $\mu > 0$ is demanded by (i), so that the surface does not oscillate below and above the tangent plane, which is implied by (ii). If the subdivision algorithm is rotationally symmetric, the subdivision matrix S is block-circulant and similar to a block-diagonal matrix.

$$S = (F_n \otimes I_m) \cdot \begin{bmatrix} \hat{S}^0 & & \\ & \ddots & \\ & & \hat{S}^{n-1} \end{bmatrix} \cdot \left(F_n^{-1} \otimes I_m\right),$$

where I_m is the $m \times m$ identity matrix with $m \cdot n = l$, $F_n = [\omega_n^{-ij}]_{i,j=0}^{n-1}$ the $n \times n$ Fourier matrix and $\otimes$ denotes the Kronecker product of two matrices $A = [a_{\nu\mu}]_{\nu,\mu}$ and B which is defined as $A \otimes B := [a_{\nu\mu} B]$. Thus, $\mathrm{spec}(S) =$

$\bigcup_i \operatorname{spec}(\hat{S}^i)$ and an eigenvalue ν of S is said to have Fourier index $f \in \mathcal{F}(\nu)$ if $\nu \in \operatorname{spec}(\hat{S}^f)$. Under conditions (i)–(iii) the Gauss curvature of a subdivision surface in the vicinity of $\mathbf{s}$ can have arbitrary sign if, see Peters and Reif (2004):

(iv) $\mathcal{F}(\mu) = \{0, 2, n-2\}$.

Condition (i) and (ii) impose linear and quadratic equality- and inequality-constraints on the eigenvalues $\lambda_0, \dots, \lambda_5$. Thus, the remaining eigenvalues λ_i can be chosen arbitrarily as long as $\lambda_5 > |\lambda_i|$ for $i = 6, \dots, l$. We will refer to the other constraints (iii) and (iv) as hard constraints.

3. The tuning method

The principle of the tuning method is based on the diagonalization of the Fourier blocks $\hat{S}^i$ and their internal block structure, see Prautzsch and Umlauf (1998, 2000). Assuming that the stencils for the vertices in the k_1-ring neighborhood of $\mathbf{c}_{r+1}$ use only vertices in the k_2-ring neighborhood of $\mathbf{c}_r$ for $k_2 \leqslant k_1 \leqslant k$, with $1 + k(k+1)/2 = m$ for triangular and $1 + k(k+1) = m$ for quadrilateral nets, the blocks $\hat{S}^i$ are lower block-triangular matrices

$$\hat{S}^i = \begin{bmatrix} \hat{S}_1^i & \\ \hat{S}_2^i & \hat{S}_3^i \end{bmatrix}.$$

The blocks $\hat{S}_1^i$ are of size $m_1 \times m_1$ and the blocks $\hat{S}_3^i$ of size $m_2 \times m_2$ with $m_1 + m_2 = m$. Now, only $\hat{S}_1^i$ will be diagonalized in order to keep the number of affected stencils as small as possible. Let $\hat{V}_1^i$ be the matrix of eigenvectors of $\hat{S}_1^i$ and $\hat{W}_1^i := (\hat{V}_1^i)^{-1}$ its inverse, then

$$\hat{W}_1^i \cdot \hat{S}_1^i \cdot \hat{V}_1^i = \operatorname{diag}\big(\lambda_1^i, \dots, \lambda_{m_1}^i\big) =: \Lambda_1^i, \quad i = 0, \dots, n-1.$$

Changing the eigenvalues λ_j^i to $\tilde{\lambda}_j^i$ for $j = 0, \dots, m_1$, changes Λ_1^i to $\tilde{\Lambda}_1^i := \operatorname{diag}(\tilde{\lambda}_1^i, \dots, \tilde{\lambda}_{m_1}^i)$, and in the sequel we will identify all variables that depend on $\tilde{\lambda}_1^i, \dots, \tilde{\lambda}_{m_1}^i$ with a tilde. So, this also changes $\hat{S}^i$ to $\tilde{\hat{S}}^i$. Separating the stencils encoded in $\hat{S}_1^i$ from the stencils encoded in $[\hat{S}_2^i \hat{S}_3^i]$ splits $\tilde{\hat{S}}^i$ into

$$\tilde{\hat{S}}^i = \tilde{\hat{A}}^i + \hat{B}^i \quad \text{with } \tilde{\hat{A}}^i = \begin{bmatrix} \tilde{\hat{S}}_1^i & 0 \\ 0 & 0 \end{bmatrix} \text{ and } \hat{B}^i = \begin{bmatrix} 0 & 0 \\ \hat{S}_2^i & \hat{S}_3^i \end{bmatrix}, \tag{1}$$

where $\tilde{\hat{A}}^i$ is assumed to be diagonalizable by

$$\tilde{\hat{A}}^i = \begin{bmatrix} \hat{V}_1^i & 0 \\ 0 & I_{m_2} \end{bmatrix} \cdot \begin{bmatrix} \tilde{\Lambda}_1^i & 0 \\ 0 & 0 \end{bmatrix} \cdot \begin{bmatrix} \hat{W}_1^i & 0 \\ 0 & I_{m_2} \end{bmatrix}.$$

Note that $\tilde{\hat{A}}^i$ depends linearly on $\tilde{\lambda}_1^i, \dots, \tilde{\lambda}_{m_1}^i$ if $\hat{V}_1^i$ does not change, while $\hat{B}^i$ does not depend on $\tilde{\lambda}_1^i, \dots, \tilde{\lambda}_{m_1}^i$ (see Section 5). Denote by $\mathbf{v}_{j,1}^i$ the columns of $\hat{V}_1^i$ and by $\mathbf{w}_{j,1}^i$ the rows of $\hat{W}_1^i$, $j = 1, \dots, m_1$. The corresponding right and left eigenvectors $\hat{\mathbf{a}}_j^i$ and $\hat{\mathbf{b}}_j^i$ of $\tilde{\hat{A}}^i$ are given by $\hat{\mathbf{a}}_j^i = [(\hat{\mathbf{v}}_{j,1}^i)^t, \mathbf{0}^t]^t$ and $\hat{\mathbf{b}}_j^i = [(\hat{\mathbf{w}}_{j,1}^i)^t, \mathbf{0}^t]$. Because of the block structure of $\tilde{\hat{S}}^i$, its eigenvalues include $\tilde{\lambda}_1^i, \dots, \tilde{\lambda}_{m_1}^i$ with corresponding left eigenvectors $\hat{\mathbf{b}}_1^i, \dots, \hat{\mathbf{b}}_{m_1}^i$. However, the right eigenvectors $\hat{\mathbf{v}}_j^i = [(\hat{\mathbf{v}}_1^i)^t, (\tilde{\hat{\mathbf{v}}}_2^i)^t]^t$ of $\tilde{\hat{S}}^i$ change. This will be discussed in detail in Section 5.

If only the eigenvalues $\tilde{\lambda}_1^i, \dots, \tilde{\lambda}_{m_1}^i$ are used for optimization, we can use a local optimization that will only affect the stencils encoded in $\tilde{\hat{S}}_1^i$. Applying the discrete inverse Fourier transform we obtain the modified subdivision matrix $\tilde{S}$ such that $\tilde{S} = \tilde{A} + B$ with

$$\begin{aligned} \tilde{A} &= (F_n \otimes I_m) \cdot \operatorname{diag}\big(\tilde{\hat{A}}^0, \dots, \tilde{\hat{A}}^{n-1}\big) \cdot \big(F_n^{-1} \otimes I_m\big), \\ B &= (F_n \otimes I_m) \cdot \operatorname{diag}\big(\hat{B}^0, \dots, \hat{B}^{n-1}\big) \cdot \big(F_n^{-1} \otimes I_m\big). \end{aligned}$$

The matrix $\tilde{A}$ now contains the stencils that are used for optimization and B contains the unchanged part of S.

4. Energy optimization

For the purpose of energy optimization the labeling of the control points C_r is changed such that the eigenvalues $\tilde{\lambda}_1^i, \ldots, \tilde{\lambda}_{m_1}^i$, $i = 0, \ldots, n-1$, of $\tilde{A}$ correspond to the first $m' = m_1 \cdot n$ rows and columns of the subdivision matrix. This is achieved by a permutation P such that $\overline{C}_r := PC_r$, $\overline{\tilde{S}'} := P\tilde{S}P^t$, $\overline{\tilde{A}} := P\tilde{A}P^t$ and $\overline{B} := PBP^t$. Then, denote by R the matrix of eigenvectors of $\overline{\tilde{A}}$, by L its inverse with rows $\mathbf{w}_0, \ldots, \mathbf{w}_l$ and by $D = \operatorname{diag}(\tilde{\lambda}_0, \ldots, \tilde{\lambda}_{m'}, 0, \ldots, 0)$ the diagonal matrix of the corresponding eigenvalues. For the optimization only the first m' eigenvalues will be modified. The matrices R, L and the remaining zero-eigenvalues of A are not changed.

For the optimization of a spline surface $\mathbf{x} : \mathbb{R}^2 \to \mathbb{R}^3$ with control points $\mathbf{p}_1, \ldots, \mathbf{p}_q \in \mathbb{R}^3$ quadratic functionals are used, see e.g. Kallay (1993), such that

$$F(\mathbf{x}) = \sum_{c=1}^{3} \left[\mathbf{p}_1^c, \ldots, \mathbf{p}_q^c\right] \cdot E \cdot \left[\mathbf{p}_1^c, \ldots, \mathbf{p}_q^c\right]^t,$$

where $\mathbf{p}_j^c$ denotes the c-th coordinate of control point $\mathbf{p}_j$. For an example see Eq. (6). The matrix E contains the energies of the spline basis functions. If $\mathbf{f}$ consists of b-spline or box-spline functions, the surface rings $\mathbf{x}_r$ consist of s polynomial patches. The energy $F(\mathbf{x}_r)$ can then be computed as

$$F(\mathbf{x}_r) = \sum_{c=1}^{3} \sum_{j=1}^{s} \left(\overline{C}_r^c\right)^t P_j^t E P_j \overline{C}_r^c = \sum_{c=1}^{3} \left(\overline{C}_r^c\right)^t \cdot \underbrace{\left(\sum_{j=1}^{s} P_j^t E P_j\right)}_{=:\, G} \cdot \overline{C}_r^c,$$

where $\overline{C}_r^c$ denotes the column vector of cth coordinates of the control points of $\overline{C}_r$. The matrices P_j select those points from $\overline{C}_r$ that define the jth patch of $\mathbf{x}_r$. Thus, the energy of $\mathbf{x}_{r+1}$ is given by

$$\tilde{F}(\mathbf{x}_{r+1}) = \sum_{c=1}^{3} \left(\overline{C}_r^c\right)^t \tilde{S}^t G \tilde{S} \overline{C}_r^c = \sum_{c=1}^{3} \left(\overline{C}_r^c\right)^t \left(\overline{\tilde{A}}^t + \overline{B}^t\right) G \left(\overline{\tilde{A}} + \overline{B}\right) \overline{C}_r^c. \tag{2}$$

The size of the matrices P_j and the number s depend on the number of polynomial patches that are affected by the optimized stencils. If for example for the algorithm of Loop the stencils for the edge points adjacent to an irregular vertex of valence n are used for optimization, two spline rings have to be considered by $F(\mathbf{x}_{r+1})$ and thus $s = 8n$. The right-hand side of Eq. (2) contains terms $\overline{\tilde{A}} \cdot \overline{C}_r^c$ which are of the form

$$\overline{\tilde{A}} \cdot \overline{C}_r^c = R \cdot D \cdot L \cdot \overline{C}_r^c = R \cdot D \cdot \begin{bmatrix} \mathbf{d}_0^c \\ \vdots \\ \mathbf{d}_l^c \end{bmatrix} = \underbrace{R \cdot \operatorname{diag}\left(\mathbf{d}_0^c, \cdot, \mathbf{d}_l^c\right)}_{=:\, M^c} \cdot \tilde{\boldsymbol{\lambda}},$$

where $\mathbf{d}_i^c$ is the cth coordinate of the so-called eigencoefficient $\mathbf{d}_i = \mathbf{w}_i \overline{C}_r$ and $\tilde{\boldsymbol{\lambda}} := [\tilde{\lambda}_0, \ldots, \tilde{\lambda}_{m'}, 0, \ldots, 0]^t$. Thus,

$$\tilde{F}(\mathbf{x}_{r+1}) = \tilde{\boldsymbol{\lambda}}^t \left(\sum_{c=1}^{3} M_c^t G M_c\right) \tilde{\boldsymbol{\lambda}} + 2\left(\sum_{c=1}^{3} \left(\overline{C}_r^c\right)^t \overline{B}^t G M_c\right) \tilde{\boldsymbol{\lambda}} + \sum_{c=1}^{3} \left(\overline{C}_r^c\right)^t \overline{B}^t G \overline{B} \overline{C}_r^c \tag{3}$$

is quadratic in $\tilde{\boldsymbol{\lambda}}$ since M^c does not depend on $\tilde{\boldsymbol{\lambda}}$, because R and L are unchanged. Subject to the constraints (i) and (ii) the quadratic equation (3) is minimized to compute the new stencils, while the hard constraints (iii) and (iv) are not changed.

It makes sense to leave the sub- and subsub-dominant eigenvalues unchanged, if we apply the energy optimization technique to a bounded curvature algorithm like the modified algorithm of Loop in Ginkel and Umlauf (2006). Then only eigenvalues smaller than μ are used to optimize the shape while bounded curvature is guaranteed by construction of the original algorithm. Then it is possible to minimize the equation by quadratic programming, because the non-linear constraint $\mu = \lambda^2$ is not affected by the minimizations and only linear constraints remain.

Remark 1. The fact that the unmodified eigenvalues in $\tilde{A}$ are zero can be used to decrease the size of the matrices in Eq. (3) by deleting the corresponding rows and columns. This makes further equality constraints for the unchanged eigenvalues unnecessary and simplifies the equation.

Remark 2. A symmetric modification such that $\tilde{\lambda}_j^i = \tilde{\lambda}_j^{n-i}$ is desirable, since it produces real-valued weights for the optimized stencils. The corresponding equality constraints can be avoided by further decreasing the size of the matrices in (3), adding up the corresponding rows and columns.

A functional that can be used for optimization, is given in Eq. (6). A large collection of other possible functionals can be found in Westgaard (2000). The evaluation of parametrization invariant measures is complex and time consuming. Therefore we focus on parameterization dependent measures as reasonable approximations for fairing purposes. First order fairness measures, which lead to minimal surface area are not well suited for the construction of fair surfaces. Curvature related second order measures are used to design approximately minimal curvature surfaces. Third order measures are related to variation of curvature and lead approximately to spherical or cylindrical shapes. Since second order measures may lead to flat surfaces, minimizing variation of curvature rather than its magnitude leads to fairer, more pleasing surfaces (Moreton and Séquin, 1994).

5. Analysis of the modified subdivision matrix

The purpose of diagonalizing only $\hat{S}_1^i$ and using only its eigenvalues $\lambda_1^i, \ldots, \lambda_{m_1}^i$ for the optimization is to modify only few stencils. But this has an impact on the eigenvectors of the complete matrix $\hat{S}^i$ as noted in Section 3. This deserves attention since the sub-dominant eigenvectors define the characteristic map, whose properties are related to C^1 regularity of the subdivision surface.

Calculating the eigenvectors $\hat{\mathbf{v}}_1^i, \ldots, \hat{\mathbf{v}}_m^i$ of $\hat{S}^i$ yields the following diagonalization:

$$\hat{S}^i = \begin{bmatrix} \hat{V}_1^i & 0 \\ \hat{V}_2^i & \hat{V}_3^i \end{bmatrix} \cdot \begin{bmatrix} \Lambda_1^i & 0 \\ 0 & \Lambda_2^i \end{bmatrix} \cdot \begin{bmatrix} \hat{W}_1^i & 0 \\ \hat{W}_2^i & \hat{W}_3^i \end{bmatrix},$$

where the right and left eigenvectors corresponding to eigenvalues of $\hat{S}_1^i$ are encoded in the columns of $[(\hat{V}_1^i)^t, (\hat{V}_2^i)^t]^t$ and the rows of $[\hat{W}_1^i, 0]$, respectively. Changing Λ_1^i to $\tilde{\Lambda}_1^i$ means changing $\hat{V}_2^i$ to

$$\begin{aligned} \tilde{\hat{V}}_2^i &= -\left[\left(\hat{S}_3^i - \tilde{\lambda}_1^i I_{m_2}\right)^{-1} \hat{S}_2^i \hat{\mathbf{v}}_{1,1}^i, \ldots, \left(\hat{S}_3^i - \tilde{\lambda}_{m_1}^i I_{m_2}\right)^{-1} \hat{S}_2^i \hat{\mathbf{v}}_{m_1,1}^i\right] \\ &= -\left[\tilde{L}_1^i \hat{S}_2^i \hat{\mathbf{v}}_{1,1}^i, \ldots, \tilde{L}_{m_1}^i \hat{S}_2^i \hat{\mathbf{v}}_{m_1,1}^i\right] \end{aligned}$$

with $\tilde{L}_j^i := (\hat{S}_3^i - \tilde{\lambda}_j^i I_{m_2})^{-1}$ for $j = 1, \ldots, m_1$. This changes also $\hat{W}_2^i$ to

$$\tilde{\hat{W}}_2^i = -\hat{W}_3^i \cdot \tilde{\hat{V}}_2^i \cdot \hat{W}_1^i,$$

but does not change the stencils encoded in the rows of $[\hat{S}_2^i, \hat{S}_3^i]$, because

$$\begin{aligned} \tilde{\hat{S}}_2^i &= \tilde{\hat{V}}_2^i \cdot \tilde{\Lambda}_1^i \cdot \hat{W}_1^i + \hat{V}_3^i \cdot \Lambda_2^i \cdot \tilde{\hat{W}}_2^i = \left(\tilde{\hat{V}}_2^i \cdot \tilde{\Lambda}_1^i - \hat{V}_3^i \cdot \Lambda_2^i \cdot \hat{W}_3^i \cdot \tilde{\hat{V}}_2^i\right) \hat{W}_1^i \\ &= \left(\tilde{\hat{V}}_2^i \cdot \tilde{\Lambda}_1^i - \hat{S}_3^i \cdot \tilde{\hat{V}}_2^i\right) \hat{W}_1^i \\ &= \left[\hat{S}_3^i \tilde{L}_1^i \hat{S}_2^i \hat{\mathbf{v}}_{1,1}^i, \ldots, \hat{S}_3^i \tilde{L}_{m_1}^i \hat{S}_2^i \hat{\mathbf{v}}_{m_1,1}^i\right] \hat{W}_1^i - \left[\tilde{\lambda}_1^i \tilde{L}_1^i \hat{S}_2^i \hat{\mathbf{v}}_{1,1}^i, \ldots, \tilde{\lambda}_{m_1}^i \tilde{L}_{m_1}^i \hat{S}_2^i \hat{\mathbf{v}}_{m_1,1}^i\right] \hat{W}_1^i \\ &= \left[\left(\tilde{L}_1^i\right)^{-1} \tilde{L}_1^i \hat{S}_2^i \hat{\mathbf{v}}_{1,1}^i, \ldots, (\tilde{L}_{m_1}^i)^{-1} \tilde{L}_{m_1}^i \hat{S}_2^i \hat{\mathbf{v}}_{m_1,1}^i\right] \hat{W}_1^i = \hat{S}_2^i, \end{aligned}$$

with $\Lambda_2^i := \operatorname{diag}(\lambda_{m_1+1}^i, \ldots, \lambda_m^i)$. So, the blocks of $\tilde{S}$ are given by

$$\tilde{S}^j = \frac{1}{n} \sum_{i=0}^{n-1} \omega_n^{ij} \cdot \begin{bmatrix} \hat{V}_1^i & 0 \\ \tilde{\hat{V}}_2^i & \hat{V}_3^i \end{bmatrix} \cdot \begin{bmatrix} \tilde{\Lambda}_1^i & 0 \\ 0 & \Lambda_2^i \end{bmatrix} \cdot \begin{bmatrix} \hat{W}_1^i & 0 \\ \tilde{\hat{W}}_2^i & \hat{W}_3^i \end{bmatrix} = \frac{1}{n} \sum_{i=0}^{n-1} \omega_n^{ij} \cdot \begin{bmatrix} \tilde{\hat{S}}_1^i & 0 \\ \hat{S}_2^i & \hat{S}_3^i \end{bmatrix}.$$

This shows that although the stencils encoded by $\hat{S}_2^i$ and $\hat{S}_3^i$ are not changed, the entries in $\tilde{\hat{V}}_2^i$ depend on $\tilde{\lambda}_j^i$, $j = 1, \ldots, m_1$.

For the standard algorithms such as the algorithm of Loop or the algorithm of Catmull–Clark the sub-dominant eigenvalue λ is located in $\hat{S}^1_1$. Therefore, the eigenvalue λ is used for optimization. The new eigenvalue $\tilde{\lambda}$ is still sub-dominant since (i) contains the corresponding constraints for the optimization. This means that for the characteristic map depending on $\tilde{\lambda}$ the analysis of regularity and injectivity is no longer valid.

However, for the algorithm of Loop, using the technique described in Umlauf (2004), Ginkel and Umlauf (2007a), the characteristic map is regular and injective if for $n \geqslant 6$ condition (i), and

$$\frac{1}{8} < \tilde{\lambda} \leqslant \frac{7 + 8\cos(2\pi/n)}{8 + 16\cos(2\pi/n)} \tag{4}$$

are satisfied. This provides an interval for $\tilde{\lambda}$, which can be incorporated into the optimization as additional linear inequality constraint. For the Catmull–Clark algorithm similar bounds can be found for $n \geqslant 5$

$$\frac{1}{3} \leqslant \tilde{\lambda} \leqslant \frac{3}{4}. \tag{5}$$

6. Tuning the algorithm of Loop

In this section the results of the tuning method applied to the algorithm of Loop are presented. For this subdivision algorithm the Fourier blocks $\hat{S}^i$ of the discrete Fourier transform of S have the form

$$\hat{S}^i = \left[\begin{array}{cc|cc|ccc} \alpha_n\delta_i & (1-\alpha_n)\delta_i & & & & & \\ 3\delta_i/8 & 3/8 + c_n^i/4 & & & & & \\ \hline \delta_i/8 & 3/8 + 3\omega_n^i/8 & 1/8 & 0 & & & \\ \delta_i/16 & 5/8 + c_n^i/8 & 1/16 + \omega_n^{-i}/16 & 1/16 & & & \\ \hline 0 & 3/8 & 1/8 + \omega_n^{-i}/8 & 3/8 & 0 & 0 & 0 \\ 0 & 3/8 + \omega_n^i/8 & 3/8 & 1/8 & 0 & 0 & 0 \\ 0 & 1/8 + 3\omega_n^i/8 & 3/8 & \omega_n^i/8 & 0 & 0 & 0 \end{array}\right] =: \left[\begin{array}{c|c|c} \hat{A}_i & & \\ \hline \hat{B}_i & \hat{C}_i & \\ \hline \hat{E}_i & \hat{F}_i & \mathbf{0} \end{array}\right],$$

where $c_n^i := \cos(2i\pi/n)$ and $\delta_0 = 1$ and $\delta_i = 0$ for $i \neq 0$. The blocks $\hat{S}^i$ consist of sub-blocks $\hat{A}_i, \hat{B}_i, \hat{C}_i \in \mathbb{C}^{2\times 2}$ and $\hat{E}_i, \hat{F}_i \in \mathbb{C}^{3\times 2}$ and the 3×3 zero-matrix $\mathbf{0}$. Thus, in multi-set notation the eigenvalues are

$$\begin{aligned} \{\lambda_1^0, \ldots, \lambda_7^0\} &= \{1, \mu_0, 1/8, 1/16, 0, 0, 0\}, \qquad \mu_0 := n\alpha_n - 3/8, \\ \{\lambda_1^i, \ldots, \lambda_7^i\} &= \{0, \mu_i, 1/8, 1/16, 0, 0, 0\}, \qquad \mu_i := 3/8 + c_n^i/4 \end{aligned}$$

for $i = 1, \ldots, n-1$. Using only λ_1^i and λ_2^i, $i = 0, \ldots, n-1$, for optimization involves just the diagonal block $\hat{A}^i$. The constraints are

$$\begin{aligned} &\lambda_1^0 = 1, \quad \mu_0 = \mu_2 = \mu_{n-2} = (\mu_1)^2, \\ &|\mu_i| < \mu_2 \quad \text{for } i = 3, \ldots, \lfloor n/2 \rfloor, \\ &|\lambda_1^i| < \mu_2 \quad \text{for } i = 1, \ldots, \lfloor n/2 \rfloor. \end{aligned}$$

Combining the bound (4) with $\mu_2 > 1/8$ to fulfill the hard constraint (iv), and adding symmetry results in

$$\begin{aligned} &1/\sqrt{8} < \mu_1 < \frac{7 + 8c}{8 + 16c}, \\ &\mu_i = \mu_{n-i} \quad \text{and} \quad \lambda_1^i = \lambda_1^{n-i} \quad \text{for } i = 1, \ldots, \lfloor n/2 \rfloor. \end{aligned}$$

The functional that has been used for the optimization is

$$F(\mathbf{x}) = \int\limits_{[0,1]^2} \left(\mathbf{x}_{uuu}^2 + 3\mathbf{x}_{uuv}^2 + 3\mathbf{x}_{uvv}^2 + \mathbf{x}_{vvv}^2\right) \mathrm{d}u\, \mathrm{d}v, \tag{6}$$

where $\mathbf{x}_u$ and $\mathbf{x}_v$ denote the partial derivatives of $\mathbf{x}$ with respect to u and v. The result of the optimization applied to the control mesh of Fig. 3 using the library (Meza, 1994) is shown in Fig. 5(a) and Table 1. In order to eliminate hybrid

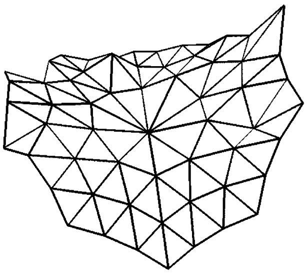

Fig. 3. Control mesh with an irregular vertex of valence 10.

Table 1
Optimized values for μ_0, μ_2, μ_{n-2} and comparison of the energies of the innermost two spline rings at the corresponding subdivision level r with and without optimization for the algorithm of Loop

r	μ_0	μ_2, μ_{n-2}	$F(\mathbf{x})$ without optimization	$F(\mathbf{x})$ with optimization
1	0.307500	0.311715	895.8735	860.4878
2	0.301400	0.306100	261.2685	244.7951
3	0.298294	0.304780	78.15931	72.64843
4	0.292570	0.304387	23.62526	21.90483
5	0.280587	0.304272	7.171128	6.643781
6	0.264509	0.304232	2.180006	2.019213
7	0.195087	0.304220	0.663041	0.614092
8	0.169850	0.304214	0.201692	0.186796
9	0.172812	0.304213	0.061355	0.056824
10	0.166834	0.304214	0.018665	0.017286

shapes, we replace the constraints $\mu_2 = \mu_{n-2} = (\mu_1)^2$ by $|\mu_2| = |\mu_{n-2}| < (\mu_1)^2$ for elliptic and $\mu_0 = (\mu_1)^2$ by $|\mu_0| < (\mu_1)^2$ for hyperbolic shapes. The influence of the optimization is visible in the visualization of the Gauss curvature. This data set shows that slight hybrid behavior of the original surface can be removed by the tuning technique. Additionally, we document the tendency towards a hyperbolic configuration in Table 1. It shows the optimized values for μ_0, μ_2 and μ_{n-2} for the first 10 subdivision steps and compares the energies of the innermost two spline rings at the corresponding subdivision level with and without optimization.

7. Tuning the algorithm of Catmull–Clark

The proposed technique can similarly be applied to modify the algorithm of Catmull–Clark. Based on the Fourier blocks $\hat{S}^i$, $i = 0, \dots, n-1$, the eigenvalues of the subdivision matrix S for the algorithm of Catmull–Clark in multi-set notation are:

$$\{\lambda_1^0, \dots, \lambda_7^0\} = \{1, \mu_\alpha^+, \mu_\alpha^-, 1/8, 1/16, 1/32, 1/64, 0, 0, 0, 0, 0, 0\},$$

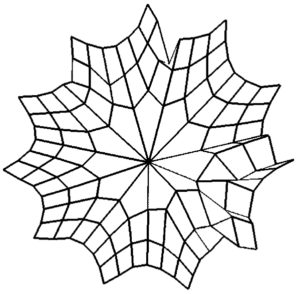

Fig. 4. Control mesh with an irregular vertex of valence 11.

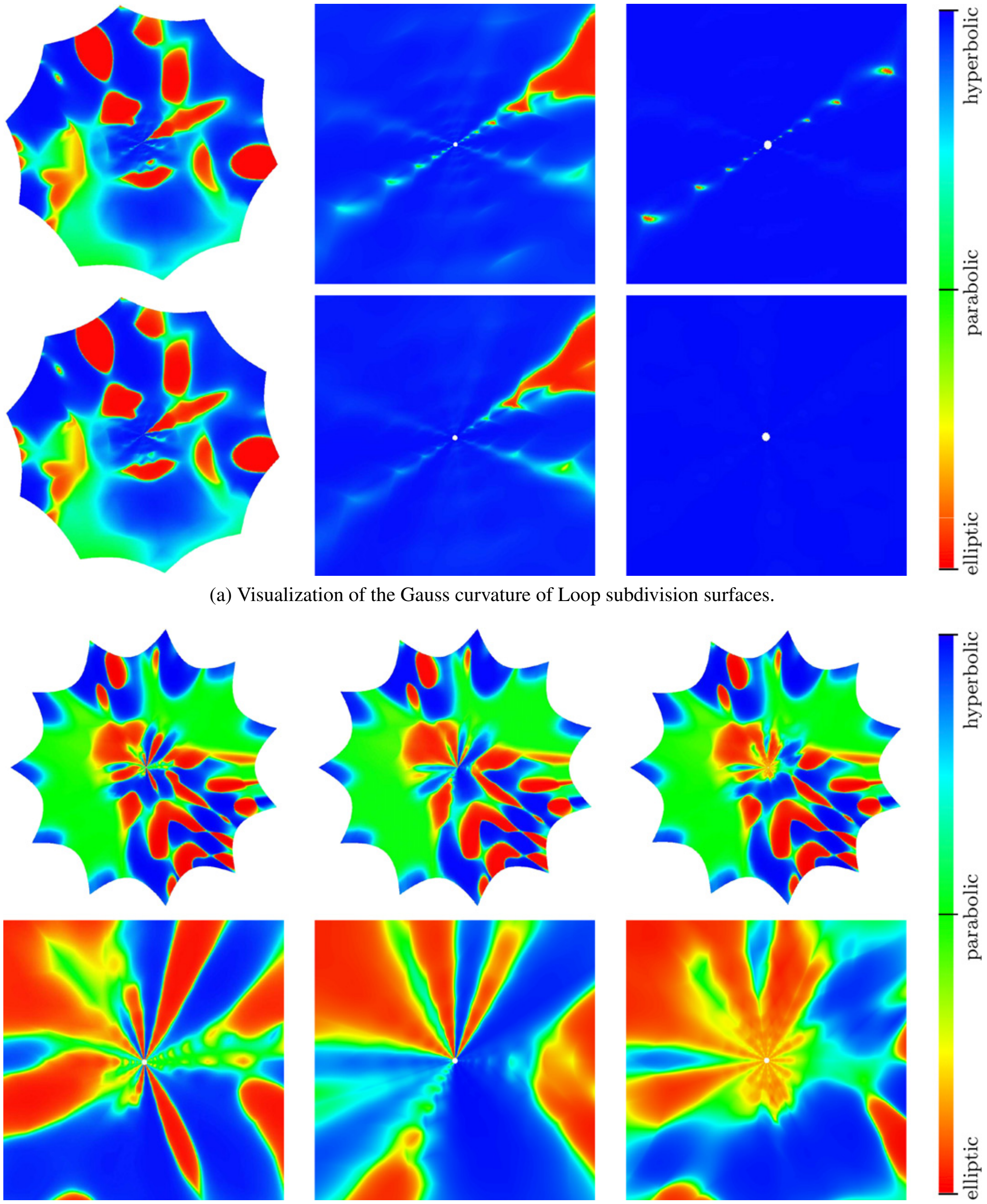

(a) Visualization of the Gauss curvature of Loop subdivision surfaces.

(b) Visualization of the Gauss curvature of Catmull–Clark subdivision surfaces.

Fig. 5. (a) Visualization of the Gauss curvature of the subdivision surface (left) computed by the modified algorithm of Loop (Ginkel and Umlauf, 2006) (top row) and the optimized subdivision algorithm (bottom row), zoom after 12 steps (middle) and 20 steps (right). (b) Comparison of three different subdivision surfaces after 12 subdivision steps. *Left*: Modified Catmull–Clark algorithm (Prautzsch and Umlauf, 1998) with bounded curvature of arbitrary sign. *Middle*: Optimized Catmull–Clark algorithm with triple subsub-dominant eigenvalue. *Right*: Optimized Catmull–Clark algorithm with single subsub-dominant eigenvalue for elliptic shape. The top row shows the surface and the bottom row shows the corresponding zoom at the extraordinary point.

$$\mu_\alpha^\pm := \left(4\alpha - 1 \pm \sqrt{(4\alpha-1)^2 + 8\beta - 4}\right)/8$$

$$\left\{\lambda_1^i, \ldots, \lambda_7^i\right\} = \{0, \mu_i^+, \mu_i^-, 1/8, 1/16, 1/32, 1/64, 0, 0, 0, 0, 0, 0\},$$

$$\mu_i^\pm := \left(5 + c_i \pm \sqrt{(c_i+9)(c_i+1)}\right)/16 \quad \text{for } i = 1, \ldots, n-1,$$

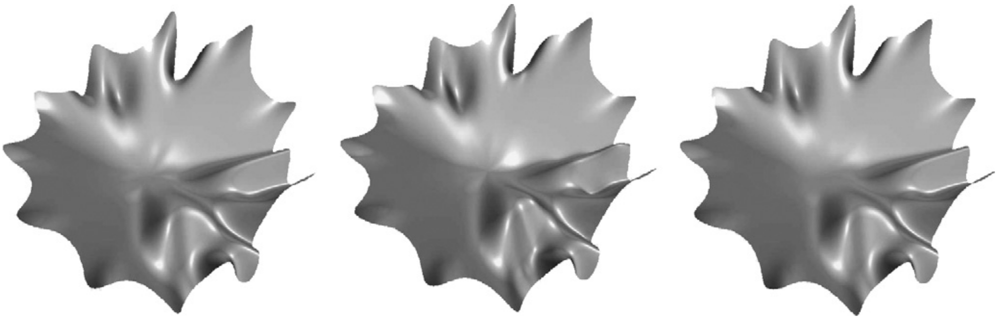

Fig. 6. The limit surfaces corresponding to the subdivision surfaces in Fig. 5(b).

with $\alpha = 1 - 7/(4n)$, $\beta = 3/(2n)$ and $c_i = \cos(2\pi i/n)$. The upper left 3×3 block of $\hat{S}_i$ corresponds to the extraordinary vertex and its one-ring neighborhood. Diagonalizing this block, its eigenvalues can be used for optimization subject to the following constraints:

$$\begin{aligned}
&\lambda_1^0 = 1,\\
&1/\sqrt{8} < \mu_1^+ < 3/4,\\
&\mu_\alpha^+ = \mu_2^+ = (\mu_1^+)^2,\\
&\mu_i^+ = \mu_{n-i}^+ \quad \text{and} \quad \mu_i^- = \mu_{n-i}^- \quad \text{for } i = 1, \dots, \lfloor n/2 \rfloor,\\
&|\mu_\alpha^-|, |\mu_i^\pm|, |\mu_1^-|, |\mu_2^-| < \mu_2^+ \quad \text{for } i = 3, \dots, \lfloor n/2 \rfloor.
\end{aligned}$$

The results of an optimization with these constraints are shown in Figs. 5(b) and 6. The control mesh shown in Fig. 4 has an irregular vertex of valence 11. The functional that has been used for the optimization is

$$F(\mathbf{x}) = \int\limits_{[0,1]^2} \left(\mathbf{x}_{uuu}^2 + 3\mathbf{x}_{uuv}^2 + 3\mathbf{x}_{uvv}^2 + \mathbf{x}_{vvv}^2\right) \mathrm{d}u \, \mathrm{d}v, \tag{7}$$

where $\mathbf{x}_u$ and $\mathbf{x}_v$ denote the partial derivatives of $\mathbf{x}$ with respect to u and v, $\Delta\mathbf{x} = \mathbf{x}_{uu} + \mathbf{x}_{vv}$ the Laplace operator and $\nabla\mathbf{x} = (\mathbf{x}_u, \mathbf{x}_v)$ the gradient of $\mathbf{x}$.

Fig. 5(b) shows that strong hybrid behavior can be decreased, but is not necessarily removed by the optimization technique using a triple subsub-dominant eigenvalue. Hybrid shapes can for example be eliminated, if we replace the constraints $\mu_2 = \mu_{n-2} = (\mu_1)^2$ by $|\mu_2| = |\mu_{n-2}| < (\mu_1)^2$. Then a surface is produced, which is elliptic in the vicinity of the extraordinary point, if the eigenvector corresponding to μ is non-hybrid and generates an elliptic central surface (Ginkel and Umlauf, 2008), see Fig. 5(b) bottom right.

References

Augsdörfer, U., Dodgson, N.A., Sabin, M.A., 2005. A new way to tune subdivision. In: Desbrun, M., Pottmann H. (Eds), Eurographics Symposium on Geometry Processing.

Barthe, L., Kobbelt, L., 2004. Subdivision scheme tuning around extraordinary vertices. Comput. Aided Geom. Design 21, 561–583.

Catmull, E., Clark, J., 1978. Recursive generated B-spline surfaces on arbitrary topological meshes. Comput.-Aided Des. 10, 350–355.

Doo, D.W.H., Sabin, M., 1978. Behaviour of recursive division surfaces near extraordinary points. Comput.-Aided Des. 10, 356–360.

Ginkel, I., Umlauf, G., 2006. Loop subdivision with curvature control. In: Polthier, K., Sheffer, A. (Eds.), Eurographics Symposium on Geometry Processing, pp. 163–171.

Ginkel, I., Umlauf, G., 2007a. Analyzing a generalized Loop subdivision scheme. Computing 79 (2–4), 353–363.

Ginkel, I., Umlauf, G., 2007b. Tuning subdivision algorithms using constrained energy optimization. In: The Mathematics of Surfaces XII, Springer, in press.

Ginkel, I., Umlauf, G., 2008. Symmetry of shape charts. Comput. Aided Geom. Design 25 (3), 131–136, this issue.

Halstead, M.A., Kass, M., DeRose, T.D., 1993. Efficient, fair interpolation using Catmull–Clark surfaces. In: SIGGRAPH '93, pp. 35–44.

Holt, F., 1996. Towards a curvature-continuous stationary subdivision algorithm. Z. Angew. Math. Mech. 76, 423–424.

Kallay, M., 1993. Constrained optimization in surface design. In: Falcidieno, B., Kunii, T.L. (Eds.), Modeling in Computer Graphics. Springer, pp. 85–93.

Karciauskas, K., Peters, J., Reif, U., 2004. Shape characterization of subdivision surfaces—case studies. Comput. Aided Geom. Design 21, 601–614.

Kobbelt, L., 1996. A variational approach to subdivision. Comput. Aided Geom. Design 13, 743–761.

Loop, C., 1987. Smooth subdivision surfaces based on triangles, Master Thesis, University of Utah.

Loop, C., 2002. Bounded curvature triangle mesh subdivision with the convex hull property. Visual Comput. 18, 316–325.

Meza, J.C., 1994. Opt++: An object oriented class library for non-linear optimization. Tech. Report 94-8225, SANDIA National Laboratories.

Moreton, H., Séquin, C., 1994. Minimum variation curves and surfaces for computer-aided geometric design. In: Sapidis, N.S. (Ed.), Designing Fair Curves and Surfaces. SIAM, Philadelphia, pp. 123–159.

Ni, T., Nasri, A., Peters, J., 2007. Ternary subdivision for quadrilateral meshes. Comput. Aided Geom. Design 24, 361–370.

Peters, J., Reif, U., 2004. Shape characterization of subdivision surfaces—basic principles. Comput. Aided Geom. Design 21, 585–599.

Peters, J., Umlauf, G., 2000. Gaussian and mean curvature of subdivision surfaces. In: Cipolla, R., Martin, R. (Eds.), The Mathematics of Surfaces IX. Springer, pp. 59–69.

Prautzsch, H., 1998. Smoothness of subdivision surfaces at extraordinary points. Adv. Comput. Math. 9, 377–389.

Prautzsch, H., Umlauf, G., 1998. A G^2-subdivision algorithm. Computing 13, 217–224.

Prautzsch, H., Umlauf, G., 2000. A G^1 and G^2 subdivision scheme for triangular nets. Int. J. Shape Model. 6, 21–35.

Reif, U., 1995. A unified approach to subdivision algorithms near extraordinary vertices. Comput. Aided Geom. Design 12, 153–174.

Sabin, M.A., 1991. Cubic recursive division with bounded curvature. In: Laurent, P.J., Le Méhauté, A., Schumaker, L.L. (Eds.), Curves and Surfaces. Academic Press, pp. 411–414.

Sabin, M.A., Barthe, L., 2003. Artifacts in recursive subdivision surfaces. In: Cohen, A., Merrien, L., Schumaker, L.L. (Eds.), Curve and Surface Fitting. Saint-Malo 2002. Nashboro Press, pp. 353–362.

Umlauf, G., 2004. A technique for verifying the smoothness of subdivision schemes. In: Lucian, M.L., Neamtu, M. (Eds.), Geometric Modeling and Computing. Nashboro Press, pp. 513–521.

Westgaard, G., 2000. Construction of fair curves and surfaces. Ph.D. Thesis, TU Berlin.

Zorin, D., 1998. Stationary subdivision and multiresolution surface representations. Ph.D. Thesis, Caltech.